ENERGY EQUIPSYS

**Energy Equipment and Systems**
www.energyequipsys.com

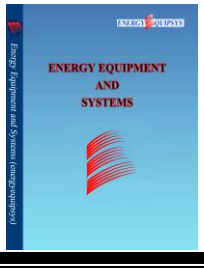


# Simulation of gas-liquid two phase flow in upriser pipe of gas-lift systems

**Pedram Hanafizadeh** [a]*
**Mahsa Moezzi** [b]
**Mohammad Hassan Saidi** [b]

[a] *Center of Excellence in Design and Optimization of Energy Systems, School of Mechanical Engineering, College of Engineering, University of Tehran, Tehran, Iran*

[b] *School of Mechanical Engineering, Sharif University of Technology, Tehran, Iran*

*Article history:*
Received 12 November 2013
Accepted 27 January 2014

**ABSTRACT**

*Gas-lift pumps are devices for lifting liquid phase incorporating the gas phase to be injected in the bottom of liquid column. They are widely used in various industrial applications such as oil extracting in petroleum industries. Gas-liquid flow being the main part of the flow through these systems, flowing in vertical pipes of gas-lift pumps has different regimes namely bubbly, slug, churn and annular. Considering each numerical method to be appropriate for modeling a certain flow regime, a suitable numerical approach is crucial to correct simulation of gas-liquid flow in upriser pipe of gas-lift systems.*

*In this paper, two main approaches namely the volume of fluid (VOF) and Eulerian model are used for modeling of the two phase flow in the upriser pipe of the airlift system. The numerical results are compared with the experimental investigations to validate the numerical models. The two phase flow regimes simulated by the numerical method were compared with the available flow regime map in the literatures. The results indicate that using the VOF is more appropriate for modeling of bubbly and slug flows while the Eulerian model fits better for only annular flow regime.*

**Keywords:** Airlift pump, Eulerian model, Numerical modelling,Two phase flow, Volume of fluid.

## 1. Introduction

Air-lift pump is a device for raising liquids or mixtures of liquids and solids through a vertical pipe, partially submerged in the liquid, by means of compressed air introduced into the pipe near the lower end. Its performance depends on two effects; differential pressure between the injection and outlet points in the pump and the influence of buoyancy force of the bubbles. The injected gas phase into the bottom of the pipe has lower density than the liquid, rises up quickly in the pipe. The liquid phase is forced to move in the same direction by the inertia of ascending gas. The main reason for rising mixture of gas-liquid to the top of the riser pipe is the lighter weight of the mixture in comparison to the liquid. Injected gas decreases the hydrostatic weight of the flow column.

The airlift pumps have important benefits, such as substantially more energy efficient for moving water under low-head condition than other pumps [1, 2], easy installation, small space requirement and ease of flow rate regulation. Using airlift pump has other advantages. Capital costs are significantly less than that for standard electrical pumps. The simplicity in its design, there are no moving parts, means that maintenance costs are also low.

These advantages accompanied by the absence of moving mechanical parts that dictate that airlift pump can be used for pumping of different fluids which are corrosive, abrasive or slurries, explosive, toxic, sandy or salty [3]. The airlift pumps are used for moving the viscous liquids like hydrocarbons in oil field industry[4], underground well drilling [3], under-sea mining [5, 6], bioreactors [7, 8]. Besides, they are used to prevent icing on high altitude [9].

White and Beardmore [10] and Zukoski [11] found out the effects of surface tension on the dynamics of vertical slug flow are very important when the tube diameter is under 20 mm. Later on, Kouremenos and Staicos [12] preformed their investigations on small diameter air lift pumps down to 12 mm diameters and low length upriser in the range of 1 to 3 m, with submergence ratios between 0.55 and 0.7.

*Corresponding author:
*Center of Excellence in Design and Optimization of Energy Systems, School of Mechanical Engineering, College of Engineering, University of Tehran, Tehran, Iran*
E-mail address: hanafizadeh@ut.ac.ir, (Pedram Hanafizadeh)

They used an equation based on momentum conservation to correlate well with the obtained measurements. They observed that the equation predicted the reverse behavior in the pump characteristic curve with experimentally observed data.Zenz [13] used various correlations to simulate airlift pumps. More recently, a wide range of investigations on the application of airlift pumps in moving liquids at nuclear fuel reprocessing plants have been realized, such as the work of de Cachard and Delhaye [14]. These studies had been mostly concerned on the accuracy of designing and modeling of the air lift pump rather than the efficiency of it. They also proposed a model to predict pressure gradient for slug flow in the airlift pump. A linear stability method was proposed by de Cachard and Delhaye [15] to consider the stability of small diameter airlift pumps. The Previous laboratory experiments [16, 17] with water and air showed that increasing the size of the injected bubbles can improve the efficiency. Most of the works that have been done on air lift pumps are experimentally [18, 19] and few numerical simulations have been performed for modeling of this type of pumping system [20, 21].

Different gas- liquid two phase flow regimes may occur in upriser pipe of airlift pumps during its operation. It is important to identify which method is appropriate for modeling of two phase flows in airlift pumps. In this study, two approaches, the volume of fluid (VOF) and Eulerian model, are used to simulate the gas- liquid two phase flow regimes in the upriser pipe of airlift pump. To compute the effect of turbulence of the flow, the k-ε model is used. Comparison of the results for VOF and Eulerian models indicates which method is more appropriate for bubbly, slug, churn and annular regimes.

## Nomenclature

| | |
|---|---|
| A | Surface area |
| C | Constant |
| D | Diameter |
| F | Force |
| g | Gravity |
| J | Superficial velocity |
| K | Interphase momentum exchange coefficient |
| k | Turbulent kinetic energy |
| K | Curvature |
| $\dot{m}$ | Mass flow rate |
| n | Surface normal |
| $p$ | Pressure |
| S | Source term |
| t | Time |
| u | Velocity |
| $v$ | Velocity |
| $V$ | Volume of phase |
| W | Mass flow rate |

### Greek letters

| | |
|---|---|
| α | Void fraction |
| ε | Turbulent dissipation |
| λ | Bulk viscosity |
| μ | Shear viscosity |
| ρ | Density |
| σ | Surface tension coefficient |
| $\phi$ | Variable |
| τ | Stress-strain tensor |

### Subscribe

| | |
|---|---|
| f | Liquid |
| g | Gas |
| $i$ | Phase of i |
| $j$ | Phase of j |
| $p$ | Primary phase |
| $q$ | Secondary phase |
| $st$ | Surface tension |
| $vm$ | Virtual mass |

## 2. Governing Equations

In this paper, two approaches, the volume of fluid (VOF) and Eulerian model were used for the numerical simulation of gas- liquid two phase flow in vertical pipe. The VOF model is applicable for modeling of two or more immiscible fluids by solving a single set of momentum equations and tracking the volume fraction of each of the fluids throughout the domain. Prediction of motion of large bubbles in a liquid and the steady or transient tracking of any gas-liquid interface are the main VOF applications.

The VOF formulation depends on the fact that two or more fluids (or phases) are not interpenetrating. In the computational cell of each control volume for each additional phase is added to the model, the volume fraction of the phase is introduced. The volume fractions of all phases sum to unity. Volume-averaged values represent that the fields for all variables and properties are shared by the phases and as long as the volume fraction of each phase is known at each location.

Therefore, the variables and properties in any given cell by considering the volume fraction values can either purely represent one of the phases or a mixture of the phases. The appropriate properties and variables will be assigned to each control volume within the domain by considering the local value of $\alpha_q$.

The Eulerian model described here is based on the two-fluid, Eulerian-Eulerian model [22, 23]. For each phase, the Eulerian modeling system is based on ensemble-averaged mass and momentum transport equations. In the present study, the liquid phase behaves as the continuum and the gaseous phase (i. e. bubbles) as the dispersed phase. The continuity equations for both Eulerian and VOF models are the same.

### 2.1. Continuity Equation

The continuity for the q[th] phase is expressed as the

$$\frac{1}{\rho_q}\left[\frac{\partial(\alpha_q\rho_q)}{\partial t}+\nabla.(\alpha_q\rho_q\overrightarrow{\upsilon_q})=\sum_{p=1}^{n}(\dot{m}_{pq}-\dot{m}_{pq})+S\right], \quad (1)$$

where $\alpha_q$, $\vec{v}_q$ and $\rho_q$ are the void fraction, velocity and density of phase q, respectively. It is assumed that mass transfer between air and water is zero ($\dot{m}_{pq}=\dot{m}_{qp}=0$). It is also supposed the source term on the right-hand side of Eq. (1), S, is zero.

The volume fraction equation will not be solved for the primary phase. So the primary-phase volume fraction will be calculated based on the constraint equation given by

$$\sum_{q=1}^{n}\alpha_q=1 \quad . \quad (2)$$

## 3. Momentum Equation for VOF model

A single momentum equation is solved throughout the domain, and then the computed velocity field is shared among the phases. The momentum equation which relies on the volume fractions of all phases is given as

$$\frac{\partial}{\partial t}\left(\rho\vec{\upsilon}\right)+\nabla.\left(\rho\vec{\upsilon}\vec{\upsilon}\right)=-\nabla p+\nabla.\left[\mu\left(\nabla\vec{\upsilon}+\nabla\vec{\upsilon}^{T}\right)\right]+\rho\vec{g}+\vec{F} \quad . \quad (3)$$

The surface tension can be expressed in terms of the pressure jump across the surface. The force at the surface can be defined as a volume force using the divergence theorem. The simplified equation of the volume force that is the source term which is added to the momentum equation is given by [24]:

$$F_{st}=\sigma_{ij}\frac{\rho\kappa_i\nabla\alpha_i}{\frac{1}{2}\left(\rho_i+\rho_j\right)} \quad . \quad (4)$$

where the properties μ is viscosity andρ is the volume-averaged density defined as

$$\alpha_G\rho_G+\alpha_L\rho_L=\rho \quad . \quad (5)$$

The curvature, k, is expressed in terms of the divergence of the unit normal, $\hat{n}$ and calculated from local gradients in the surface normal at the interface. That is,

$$k=\nabla\cdot\hat{n}=\frac{1}{|n|}\left[\left(\frac{n}{|n|}\cdot\nabla\right)|n|-\left(\nabla\cdot n\right)\right] \quad , \quad (6)$$

$$\hat{n}=\frac{n}{|n|} \quad , \quad (7)$$

where n is the surface normal and is obtained using the gradient of $\alpha_q$, the volume fraction of the q[th] phase [24]. That is,

$$n=\nabla\alpha_q \quad . \quad (8)$$

### 3.1. Momentum Equation for Eulerian-Eulerian model

The conservation of momentum for Eulerian model in multiphase flow is obtained by the volume averaged momentum equation as [22]

$$\begin{aligned}&\frac{\partial}{\partial t}(\alpha_q\rho_q\vec{v}_q)+\nabla.(\alpha_q\rho_q\vec{v}_q\vec{v}_q)\\&=-\alpha_q\nabla p+\nabla.\bar{\bar{\tau}}_q+\alpha_q\rho_q\vec{g}\\&+\alpha_q\rho_q(\vec{F}_q+\vec{F}_{lift,q}+\vec{F}_{vm,q})\\&+\sum_{p=1}^{n}(K_{pq}(\vec{v}_p-\vec{v}_q)+\dot{m}_{pq}\vec{v}_{pq})\end{aligned} \quad , \quad (9)$$

where, $\bar{\bar{\tau}}_q$ denotes the phase stress-strain tensor, $\vec{g}$is the acceleration due to gravity, $\vec{F}_q$ is an external body force, $\vec{F}_{lift,q}$ and $\vec{F}_{vm,q}$ are a lift force and a virtual mass force, respectively. Parameter P is the pressure shared by all phases and $K_{pq}$ is the interphase momentum exchange coefficient. $\vec{v}_{pq}$ Expresses the interphase velocity, which is defined the velocity of the phase transferred to the other phase. It is assumed that there is no drift flux between two phases, therefore interphase velocity is set to zero. The phase stress-strain tensor is given by

$$\bar{\bar{\tau}}_q=\alpha_q\mu_q\left(\nabla\vec{v}_q+\nabla\vec{v}_q^{T}\right)+\alpha_q\left(\lambda_q-\frac{2}{3}\mu_q\right)\nabla.\vec{v}_q\bar{\bar{I}} \quad , \quad (10)$$

where $\mu_q$ and $\lambda_q$ represent the shear and bulk viscosities of phase q, respectively. In the primary phase flow field, lift forces which mainly act on a bubble are caused by velocity gradients. The lift force will be more noticeable for large bubbles. Therefore, the inclusion of lift forces is not applicable for very small bubbles or closely packed bubbles. The lift force is calculated by [25]

$$\vec{F}_{lift}=-0.5\rho_q\alpha_p(\vec{v}_q-\vec{v}_p)\times(\nabla\times\vec{v}_q) \quad . \quad (11)$$

Virtual mass occurs when a secondary phase accelerates relative to the primary phase in multiphase flows, and is defined by [25]:

$$\vec{F}_{vm} = 0.5\alpha_q\rho_q\left(\frac{d_q\vec{v}_q}{dt} - \frac{d_p\vec{v}_p}{dt}\right), \quad (12)$$

where, the term $d_q/dt$ represents the phase material time derivative using the form

$$\frac{d_q(\phi)}{dt} = \frac{\partial(\phi)}{\partial t} + (\vec{v}_q.\nabla)\phi \quad . \quad (13)$$

Although, the primary phase density is greater than the secondary phase, the relative velocity and acceleration between the phases are not high enough. Therefore, the effect of virtual mass is not important. Increasing the computational cost, unstable the numerical solution and decreasing the solution convergence are caused by incorporating of virtual mass in governing equations. Hence, the effect ofvirtual mass is negligible in this research.

### 3.2. Turbulence Model

In the present work, turbulence is taken into account for the continuous phase. Although, the dispersed gas phase is modeled as laminar flow, the influence of the dispersed phase on the turbulence of the continuous phase is taken into consideration with Sato's additional term [26]. In order to model turbulence of the liquid phase in Eulerian-Eulerian multiphase simulations the well-known single-phase turbulence models are usually used. In the present case, the most common model is the standard k-ε model which is used for both Eulerian and VOF models [27]. The governing equations for the turbulent kinetic energy k and turbulent dissipation ε are given as

$$\begin{aligned}&\frac{\partial}{\partial t}(\alpha_q\rho_q k_q) + \nabla.(\alpha_q\rho_q\vec{U}_q k_q)\\ &= \nabla.\left(\alpha_q\frac{u_{t,q}}{\sigma_k}\nabla k_q\right) + (\alpha_q G_{k,q} - \alpha_q\rho_q\epsilon_q)\\ &+\sum_{p=1}^{N}K_{pq}(C_{pq}k_1 - C_{qq}k_q) - \sum_{p=1}^{N}K_{pq}(\vec{U}_p - \vec{U}_q).\frac{\mu_{t,p}}{\alpha_p\sigma_p}\nabla\alpha_t\\ &+\sum_{p=1}^{N}K_{pq}(\vec{U}_p - \vec{U}_q).\frac{\mu_{t,q}}{\alpha_q\sigma_q}\nabla\alpha_q \end{aligned} \quad (14)$$

$$\begin{aligned}&\frac{\partial}{\partial t}(\alpha_q\rho_q\epsilon_q) + \nabla.(\alpha_q\rho_q\vec{U}_q\epsilon_q) = \nabla.\left(\alpha_q\frac{u_{t,q}}{\sigma_\epsilon}\nabla\epsilon_q\right)\\ &+\frac{\epsilon_q}{k_q}\left[C_{1\epsilon}\alpha_q G_{k,q} - C_{2\epsilon}\alpha_q\rho_q\epsilon_q + C_{3\epsilon}\left(\begin{array}{l}\sum_{p=1}^{N}K_{pq}(C_{pq}k_p - C_{qq}k_q)\\ -\sum_{p=1}^{N}K_{pq}(\vec{U}_p - \vec{U}_q).\frac{\mu_{t,p}}{\alpha_p\sigma_p}\nabla\alpha_t\\ +\sum_{p=1}^{N}K_{pq}(\vec{U}_p - \vec{U}_q).\frac{\mu_{t,q}}{\alpha_q\sigma_q}\nabla\alpha_q\end{array}\right)\right], \end{aligned} \quad (15)$$

where $C_{pq}$ and $C_{qp}$ are defined using

$$C_{pq} = 2, C_{qp} = 2\left(\frac{\eta_{pq}}{1+\eta_{pq}}\right), \quad (16)$$

and $\eta_{pq}$ is calculated from the following equation [28]:

$$\eta_{pq} = \frac{\tau_{t,pq}}{\tau_{F,pq}} \quad . \quad (17)$$

The Lagrangian integral time scale calculated along bubble trajectories, defined as

$$\tau_{t,pq} = \frac{\tau_{t,q}}{\sqrt{(1+C_\beta\xi^2)}} \quad , \quad (18)$$

where in this equation ξ is given by

$$\xi = \frac{|\vec{v}_{pq}|\tau_{t,q}}{L_{t,q}} \; and \; C_\beta = 1.8 - 1.35\,cos^2\theta \quad , \quad (19)$$

and θ denotes the angle between the mean bubble velocity and the mean relative velocity. The detail of calculation of these terms is available in the work of Csanady [28].

The characteristic bubble relaxation time corresponding to inertial effects acting on a dispersed phase p is defined using

$$\tau_{F,pq} = \alpha_p\rho_p K_{pq}^{-1}\left(\frac{\rho_p}{\rho_q} + C_V\right). \quad (20)$$

## 4. Geometry and Grid Mesh Specification

In the present work, the two phase flow in upriser pipe of an airlift pump with a riser length of 1 m and diameter of 5 cm is considered. There are also three circular geometries at the injection port of air flow. In the first one there is a circular hole with diameter of 1cm at the center of air injector plate. In the second one, 5 circular holes with diameter of 1cm have been considered. The last one has a circular hole at the center of pipe with the same surface area of 5 holes. The schematic geometries of the vertical pipe with their applied meshing are shown in Fig. 1. In the present work, the domain of solution is selected in a manner that boundaries are conformed on cylindrical coordinate system, also, the mesh lines divide the geometry span to control volume forming the hexahedral sector. The schematic of this control volume is illustrated in Fig.2.

To validate grid independency of the results from mesh cell number, four meshes namely 40000, 50000, 58000 and 72000 hexahedral cells have been applied and pressure distribution of the two phase flow along the axial of upriser have been compared in Fig.3a and 3b. These figures show that the mesh arrangement of 58000 nodes meets the requirement of mesh independency of the results for the pressure of upriser pipe and therefore these arrangements utilized to simulate the two phase flow.

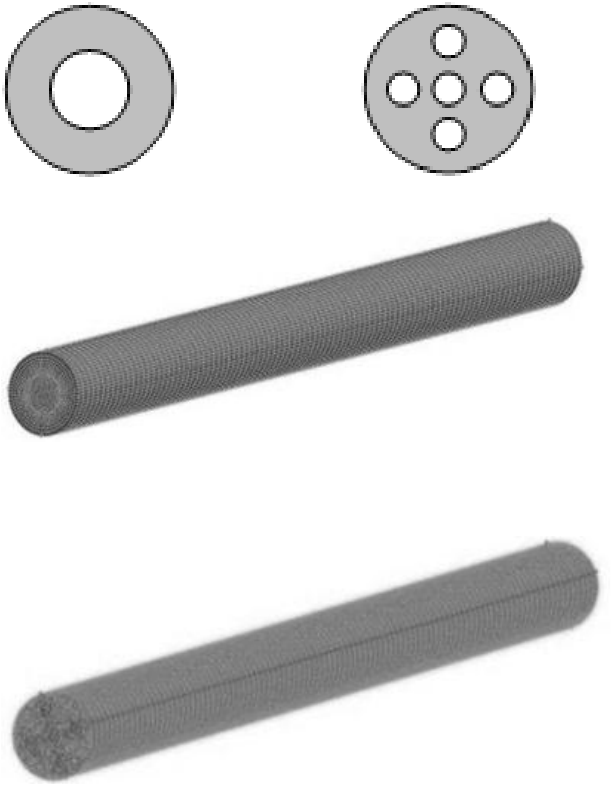

**Fig.1.** Schematic upriser pipes with applied meshing and respective air entrance geometries

Table 1 expresses the information of grid mesh that has been applied for numerical modeling.

The comparison of the numerical work has been done with experimental data of pressure distribution along the axis of 6 m vertical pipe in two phase bubbly flow for inlet air volume fraction of 0.1 to validate the numerical model and was depicted in Fig. 3c.

**Table1.** Information of applied mesh

| | |
|---|---|
| Cells | 58000 |
| Faces | 176580 |
| Nodes | 60701 |
| Minimum volume (m3) | 2.0937e-09 |
| Maximum volume (m3) | 1.365451e-07 |

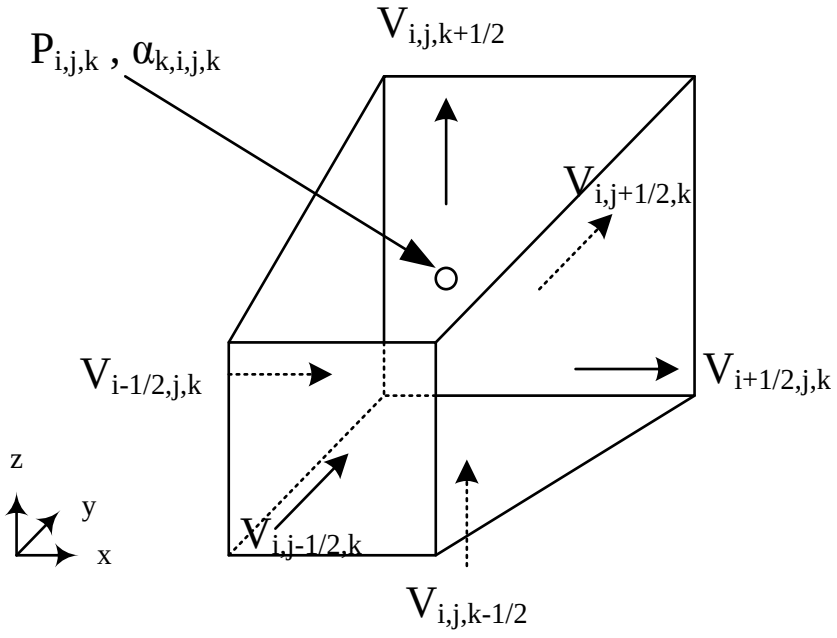


**Fig.2.** A schematic of the control volume

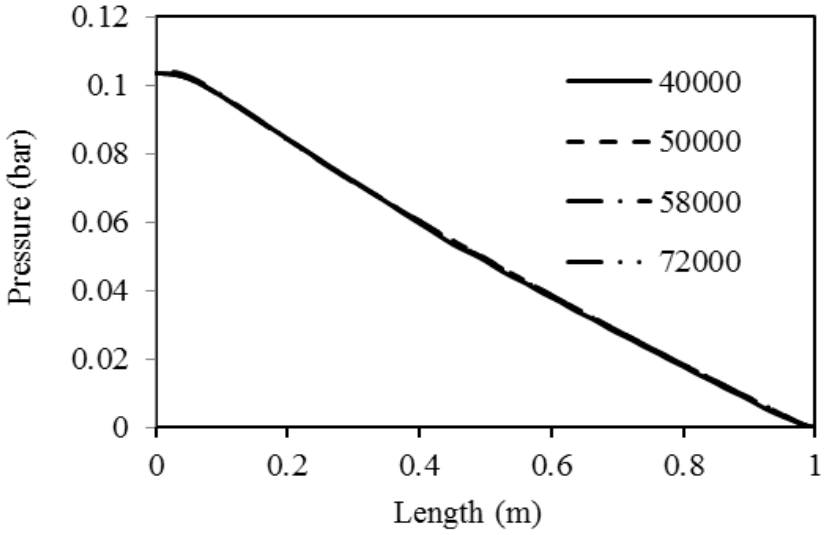


a)

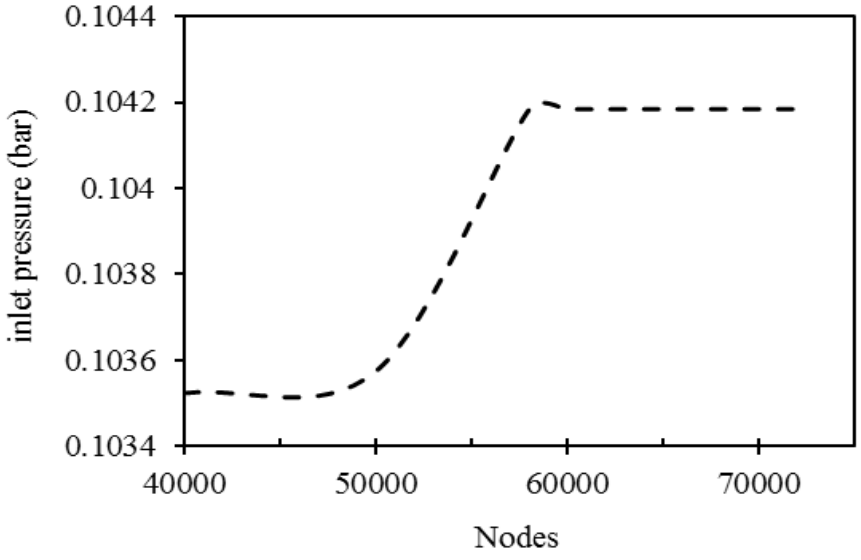


b)

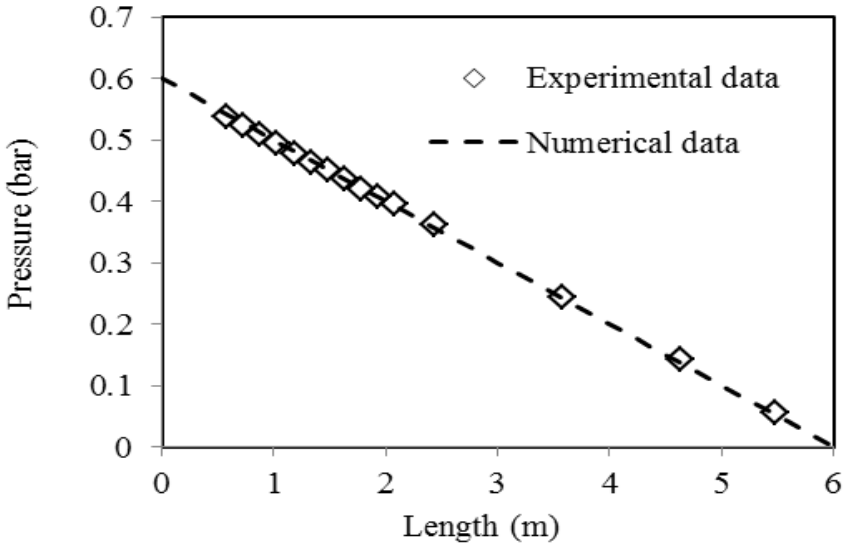


c)

**Fig.3.** a) Mesh independency diagram, b) Inlet pressure versus number of nodes,
c) Comparison of numerical results with experimental data for pressure along the axis of vertical pipe

## 5. Numerical solution method

In this study, the numerical modeling of gas- liquid flow is performed via commercial CFD package. The discretization of the governing equations, are based on the control volume frame work which is proposed by Patankar [29]. A collocated grid is used to all variables are stored at the center of control volume. Such a collocated arrangement of the mesh can represent accurate flux and source term. The governing equations are solved using the SIMPLE algorithm. The details of discretization are found in Fogt's research [30]. In order to increase the stability of the numerical solution, the time dependent equations are solved.

The system of two continuities and two momentum equations with the transport equations of turbulent energy and dissipation are solved for any iteration. Turbulent variables and velocity near the wall of the control volume are estimated from the wall laws. Velocities of both phases are calculated from the respective momentum equations and also pressure from the liquid continuity equation. Volume fraction is computed from the continuity equation of the gas phase. The two phases have been assumed as incompressible and not miscible. Gravity has been taken into account. There is also assumed no mass transfer between two phases and turbulence has been taken into account by the use of the $k$–ε model approach. The pressure-based solver was used. Constant velocities are imposed as boundary conditions at the liquid and gas inlets, while a constant outflow at the outlet. Discretization scheme for pressure and volume fraction are changed to PRESTO and Geo-Reconstruct respectively in VOF model in comparison with Eulerian.

## 6. Results

Several velocities were considered for the inlet of the air and water to create the various gas- liquid two phase flow regimes in the pipe. All these conditions were modeled with both Eulerian and VOF models to compare the result of their simulations. Figures 5, 8 and 11 illustrate the comparison of these two models which were implemented on the air-water vertical co-current two phase flow. Each figure carries out the Phase contour and contains the difference between Eulerian and VOF methods simulations for various water and air velocities inlet. These figures reveal that the VOF model can predict the bubbly, slug and churn better than the Eulerian model. In the VOF model the interface of the gas and liquid phases was simulated well. In the Eulerian model, the interface of the two phases cannot achieve. In this model, the separate bubbles were considered as a unified region with lower void fraction. This means that in the Eulerian model the simulation of the gas phase region is illustrated as a stripe. The color and the width of this stripe depend on the gas phase void fraction. Increase in the inlet gas phase increases the gas phase void fraction and the flow regime changes from bubbly to annular.

The three different air injection geometries used in this research, could contribute to investigate the effect of varying the injection ports. The appropriate numerical methods for modeling a certain flow regime have been considered by choosing a suitable numerical approach to correct simulation of gas-liquid flow in upriser pipe of airlift systems. In order to investigate results, independence of entrance effect, a test section was chosen between the heights of 0.7 to 0.8 m of the upriser to monitor all variables. This test section divided to 6 longitudinal sections and each surface section divided to 9transverse lines. By calculating volume fraction in the heights of 0.7 m to 0.8 m of the pipe, 9 transverse lines have been defined on any of such surfaces which are located in 0.02 m distance from each other, see Fig.4.

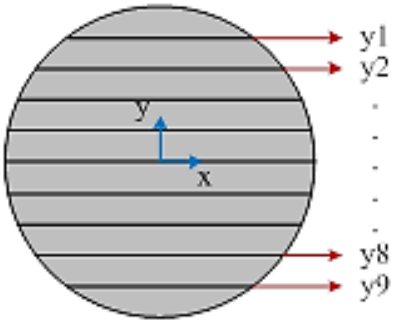


**Fig.4.** Divided surface into 10 sections

Following figures prove the variation of volume fraction have been drawn for two conditions: in length of 0.7 m for 9 lines $y_1$ to $y_9$ (Figs. 6, 9, 12) and between length of 0.7 m to 0.8 m just for line of $y_5$ (Figs. 7, 10, 14, 15, 18, 19). Calculation of $\alpha_{net}$ results in the amount value of $W_g$, $W_f$, $A_g$,$A_f$, $U_g$ and $U_f$ finally to obtain the value of superficial velocity of water ($j_f$) and air ($j_g$) in order to validate the results with the flow regime map of Taitel *et al.*[31].Figure 5 shows the phase contours of air-water two phase flow for both Eulerian and VOF models. Velocities of both phases are 0.1 m/s which create bubbly flow regime into the pipe. Despite of the Eulerian weak result, the VOF model presents well bubbly as a flow regime. Eulerian model only displays the narrow strip for gas phase while the VOF exactly shows the formed separated bubbly in flow.

Considering the result of void fraction calculation, the superficial velocity of the air and water phases have been obtained $J_g$ =0.004 m/s and $J_f$ = 0.09 m/s, respectively. The flow regime map confirms the bubbly regime as well.

Figure 6 depicts the variation of volume fraction versus x-direction in different y positions in height of 0.7m.As it demonstrates line $y_4$ has the maximum value of volume fraction in cross section of height 0.7 m. According to bubbly regime flow in this condition which was obtained by calculations and the result of simulation (Fig. 5), the existence of bubbles near the center of pipe is more than other positions in this height. The zero value of volume fraction for lines $y_1$, $y_2$, $y_8$ and $y_9$ indicates that near the wall there is almost no bubble existence.

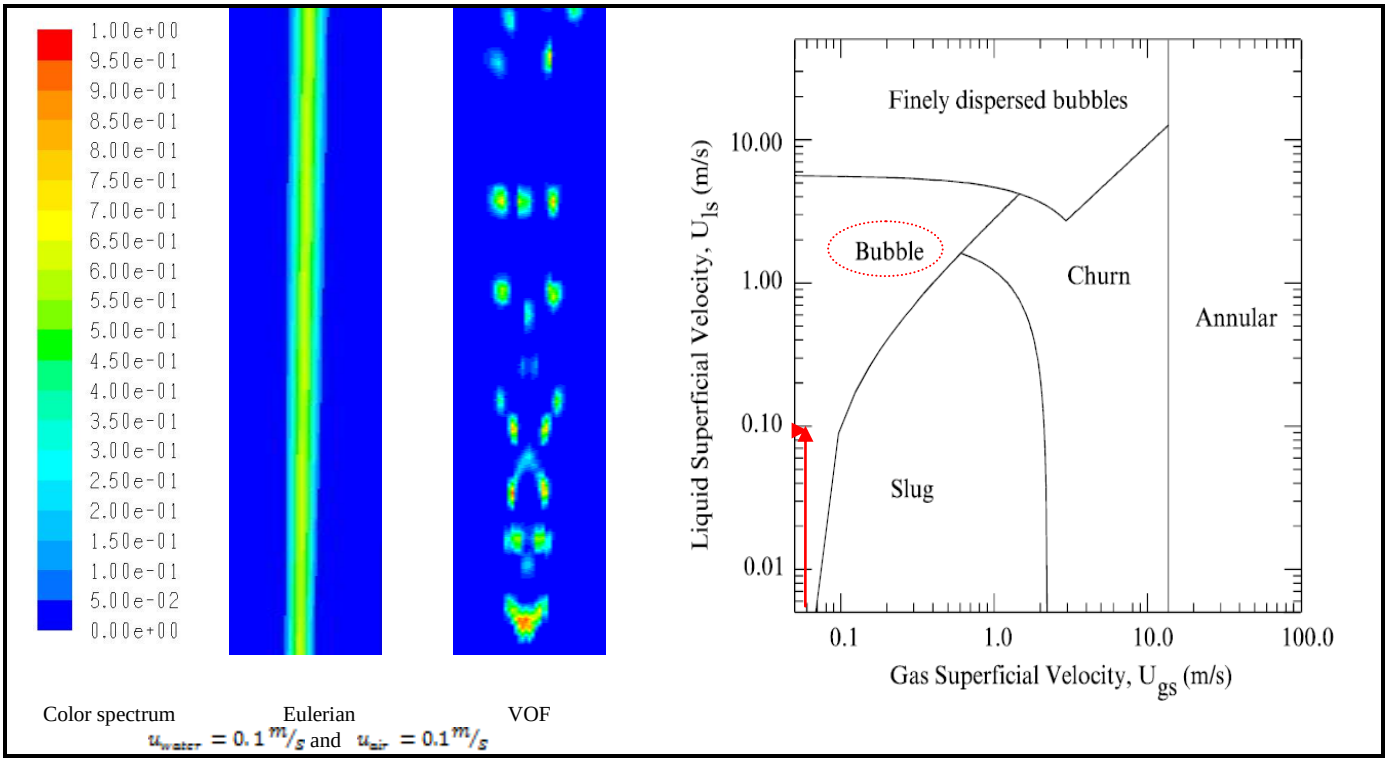


**Fig.5.** Comparison of VOF and Eulerian methods

Figure 7 shows the variation of volume fraction on the diameter in different height positions of the upriser in the range of 0.7m to 0.8m. The figure presents the maximum value of around 0.6 for volume fraction while the majority of curves in this figure have the value of less than 0.4. In this case the calculated mean value of 0.04 for volume fraction confirms such state. There are some curves with zero volume fractions that show almost no bubble exists in those locations. It expresses bubbles are dispersed in different positions of the pipe.

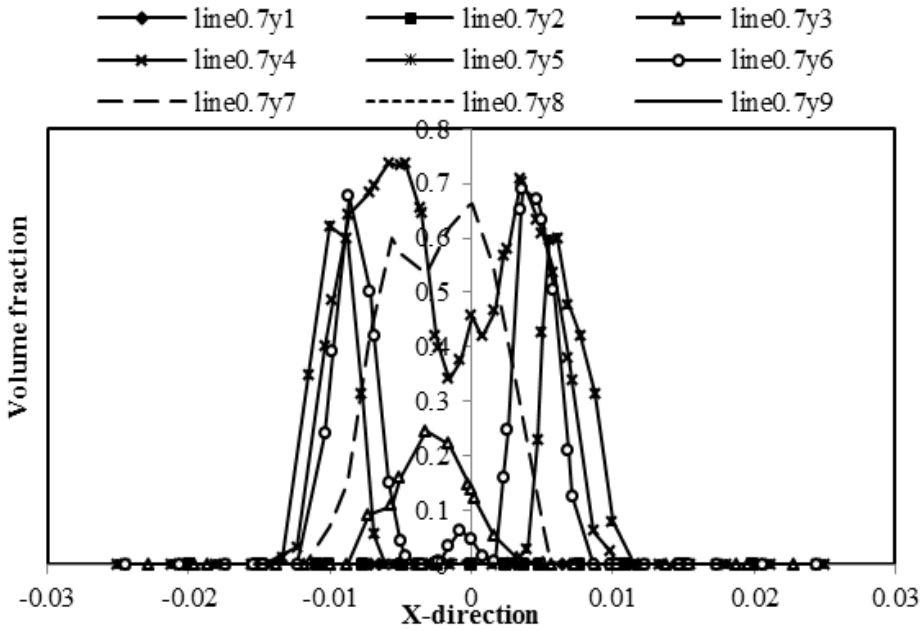


**Fig.6.** Variation of volume fraction in length of 0.7m

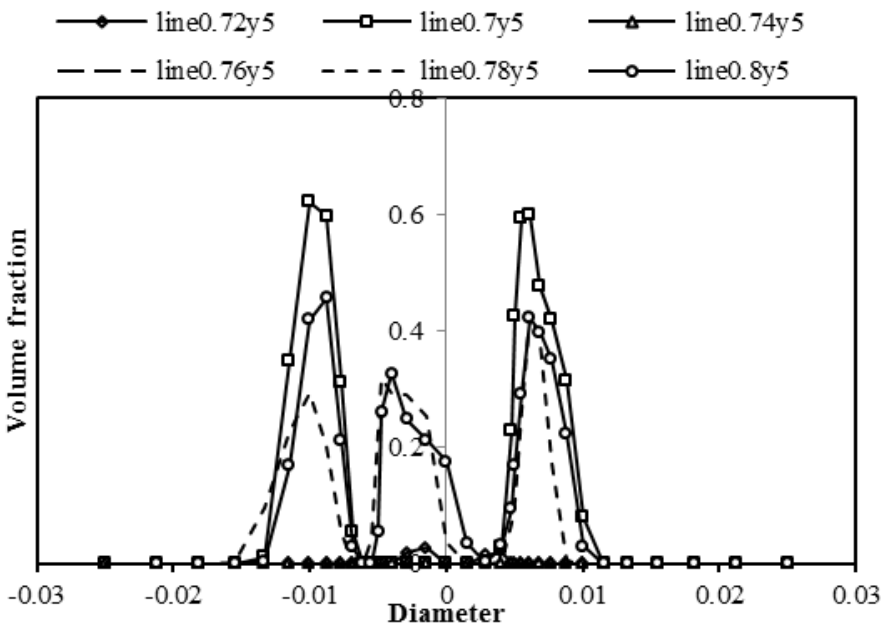


**Fig.7.** Variation of volume fraction in height of o.7m to 0.8m

Figure 8 shows the phase contours for the air injection port with 5 holes for Eulerian and VOF models.

It is obvious that the air bubbles distribute better than the one air hole injection port (Fig. 5). VOF model shows the formed separated bubbles in the flow and presents well bubbly as a dominant flow regime while Eulerian model only displays narrow strips for gas phase. The calculated result for the superficial velocity of air and water phases, $J_g$=0.01987 m/s and $J_f$= 0.08 m/s, confirms the bubbly flow as a regime of two phase flow.

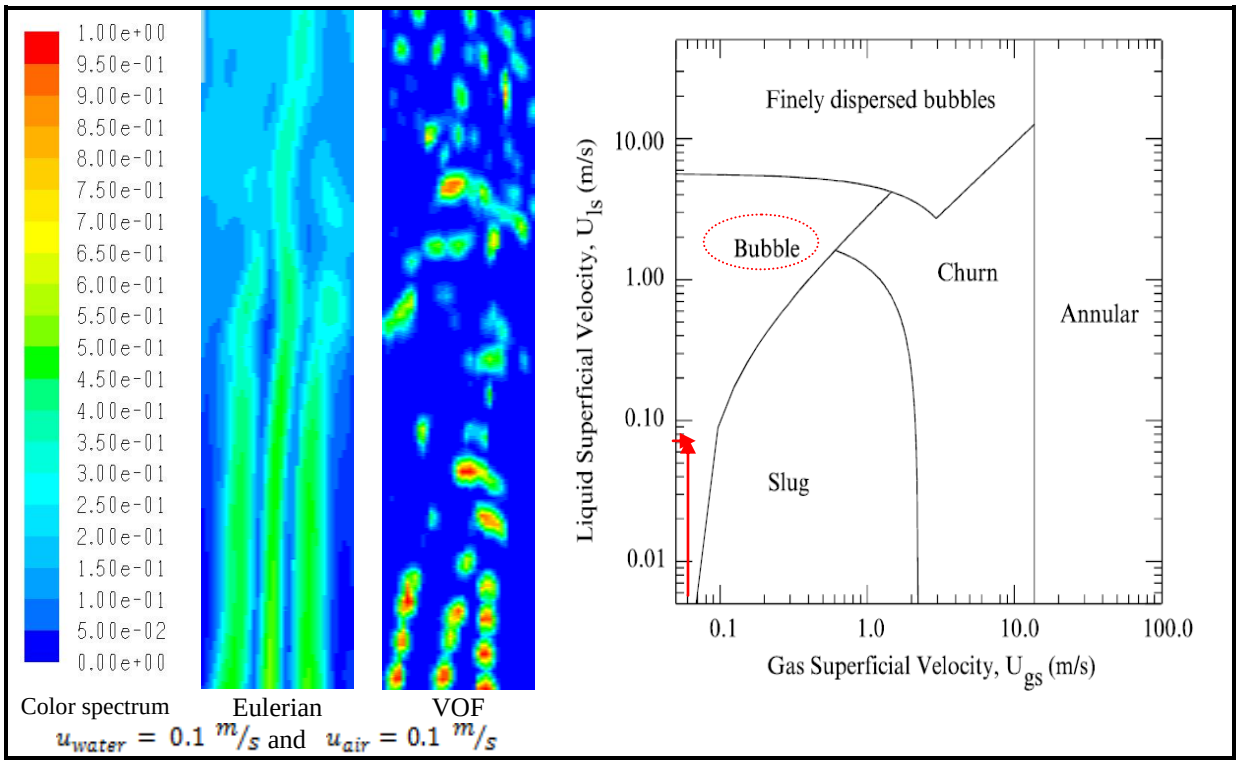


**Fig.8.** Comparison of VOF and Eulerian methods

Figure 9 shows the variation of volume fraction in different y positions in the pipe cross section at height of 0.7 m. As it demonstrates line $y_7$ has the maximum value of volume fraction between 0.8 and 0.9. Comparing with the previous sets of air inlet geometries (i.e. the pipe with one small hole at the center, Fig. 6), Fig.9 shows greater amount of volume fraction for all curves at the height of 0.7 m. The reason of such proliferation is increasing the number of air inlets to 5 holes. In addition, according to bubbly regime flow in this condition which was obtained by calculations and also the result of simulation (Fig. 8), accumulation of bubbles is not limited to the center of pipe. It means that bubbles are scattered more uniformly throughout the pipe in comparison with previous sets of study in which more bubbles were found at the center of the pipe.

Figure 10 shows the variation of volume fraction on the pipe diameter in different height positions in range of 0.7 m to 0.8 m. In comparison with the previous sets of study in which the majority of volume fraction for most curves far from the center of pipe had value of zero, Fig. 7;in here, almost these curves have non zero value in different positions even far from the center of the pipe. It expresses, bubbles exist in wider positions of the pipe even in different length same as the above curves that show the accumulation of bubbles in wider places at just length of 0.7 m. On the whole bubbles distribute in the pipe more uniformly than the pipe with one injection hole port.

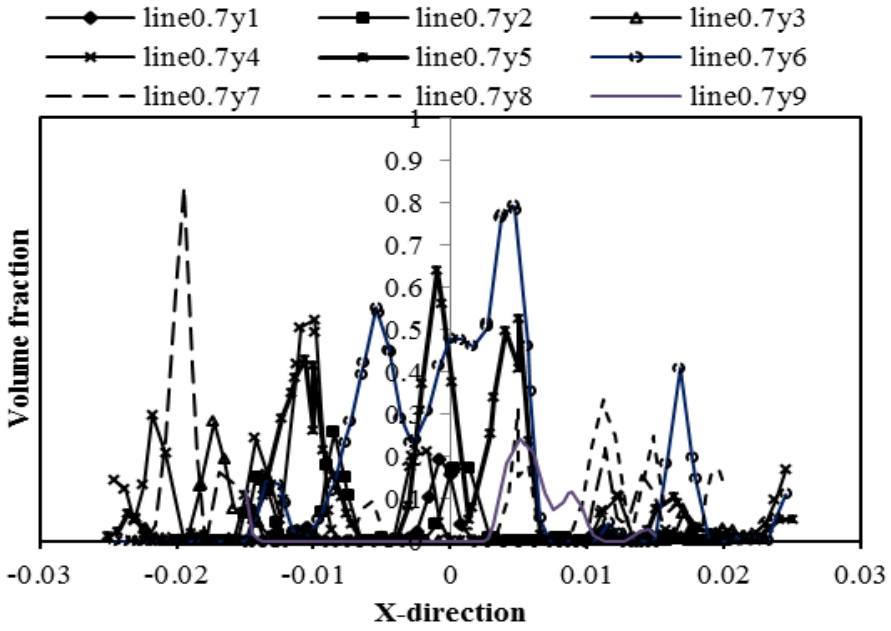


**Fig.9.** Variation of volume fraction in length of 0.7m

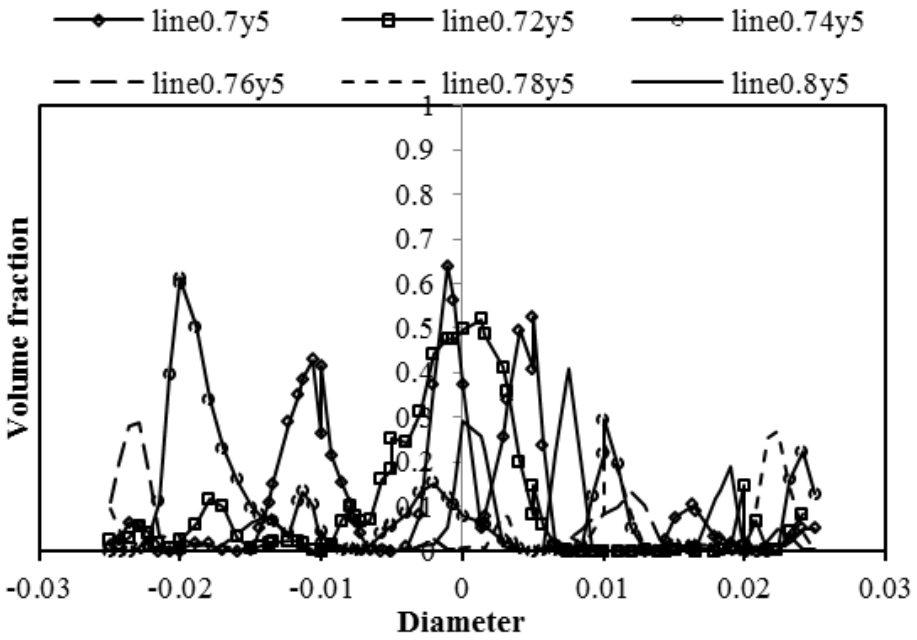


**Fig.10**.Variation of volume fraction in height of o.7m to 0.8m

Figure 11 illuminates the phase contours for one hole air injection port with the same area of the 5 holes injection port. The calculated superficial velocities of air and water phases, $J_g$ = 0.01999 m/s and $J_f$ = 0.07996 m/s, respectively indicate bubbly flow regime on the map. The VOF simulation illustrates bubbly flow, while the Eulerian simulation cannot predict this flow regime well. Despite of the bubbly flow, obtained from the pipe with a small hole at the center (See Fig. 5), here bubbles are bigger and distributed in the wider positions.

Figure 12 shows the variation of volume fraction in different y positions in height of 0.7m for one big hole injection port when the inlet velocities of water and air are $u_{water} = 0.1\ ^{m}/_{s}$ and $u_{air} = 0.1\ ^{m}/_{s}$, respectively. As the area of the injection port is equal with the area of the 5 holes injection port, the air mass flow rate for these two injection ports will be equal but greater than the one small injection port (Fig. 5). In this figure, line $y_3$ and $y_4$ have the maximum value of volume fraction between the value of 0.8 and 0.9. Despite of the previous sets of air inlet geometries including 5 holes in which bubbles have been distributed in different wide positions of the pipe, in this model distribution of bubbles is almost limited near the center of the pipe in length of 0.7m.

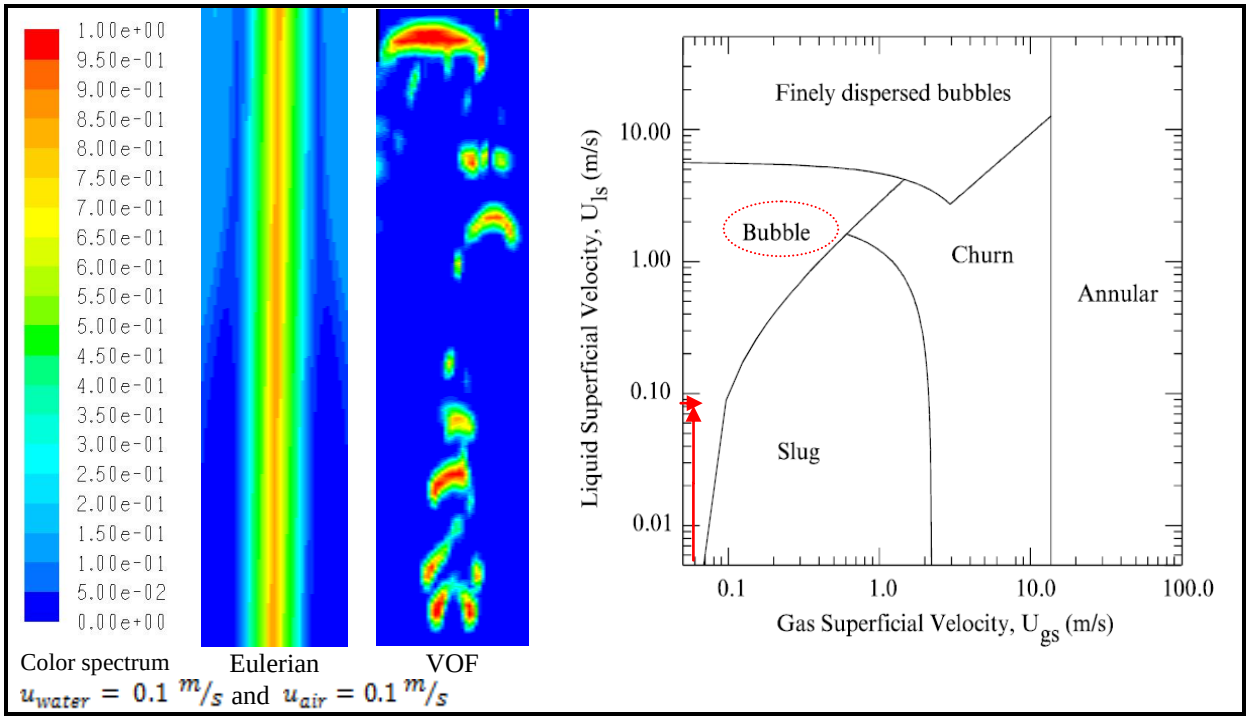


**Fig.11.** Comparison of VOF and Eulerian methods

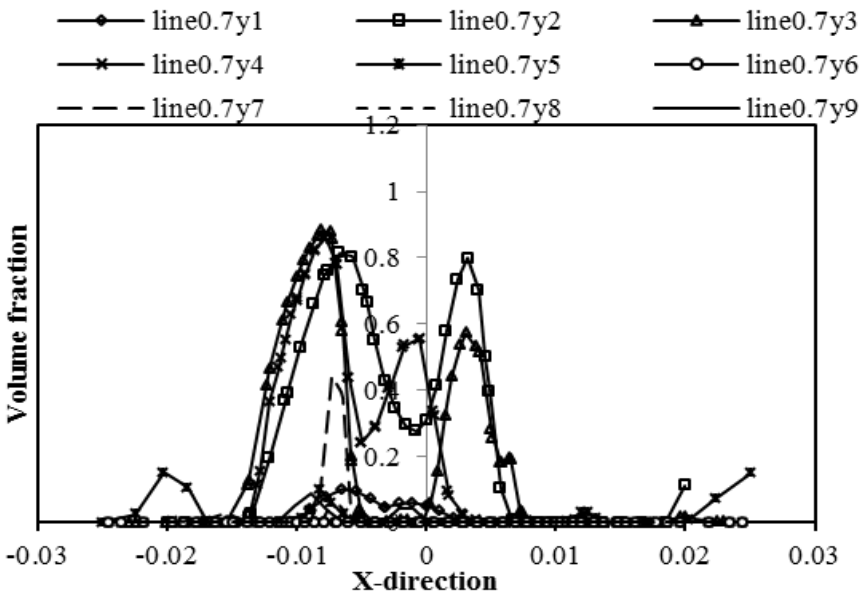


**Fig.12.** Variation of volume fraction in length of 0.7m

As the previous simulations indicate the VOF model can predict the flow regime better than the Eulerian one. So in this section the VOF simulations are applied for the both one and five holes injection port to evaluate the effect of the injection geometry on the flow regime. The VOF phase contours are illustrated in Fig.13. The inlet air and water velocities are 0.5 m/s and therefore the superficial velocities of the air and water phases will be, $J_g$ =0.09 m/s and $J_f$ = 0.4 m/s respectively. The result shows that accumulation of bubbles in five holes is not limited to the center of the pipe. It means bubbles are located in more positions of the pipe in comparison to air inlet geometries with one hole which are found more at the center of the pipe.

Comparing to the Figs.8 and 11, increasing the inlet velocities of air and water makes the size of bubbles bigger: in addition, the color of air phase will situate in an upper place in the color spectrum.

The variation of volume fraction in different height positions in range of 0.7 to 0.8m were shown for one and five holes air injection ports in Figs.14 and 15 respectively. The inlet air velocities for both phases and both injection geometries are 0.5 m/s. Figures indicate that the distribution of bubbles in one hole is concentrated in the center of the pipe and is more symmetric than the five holes.

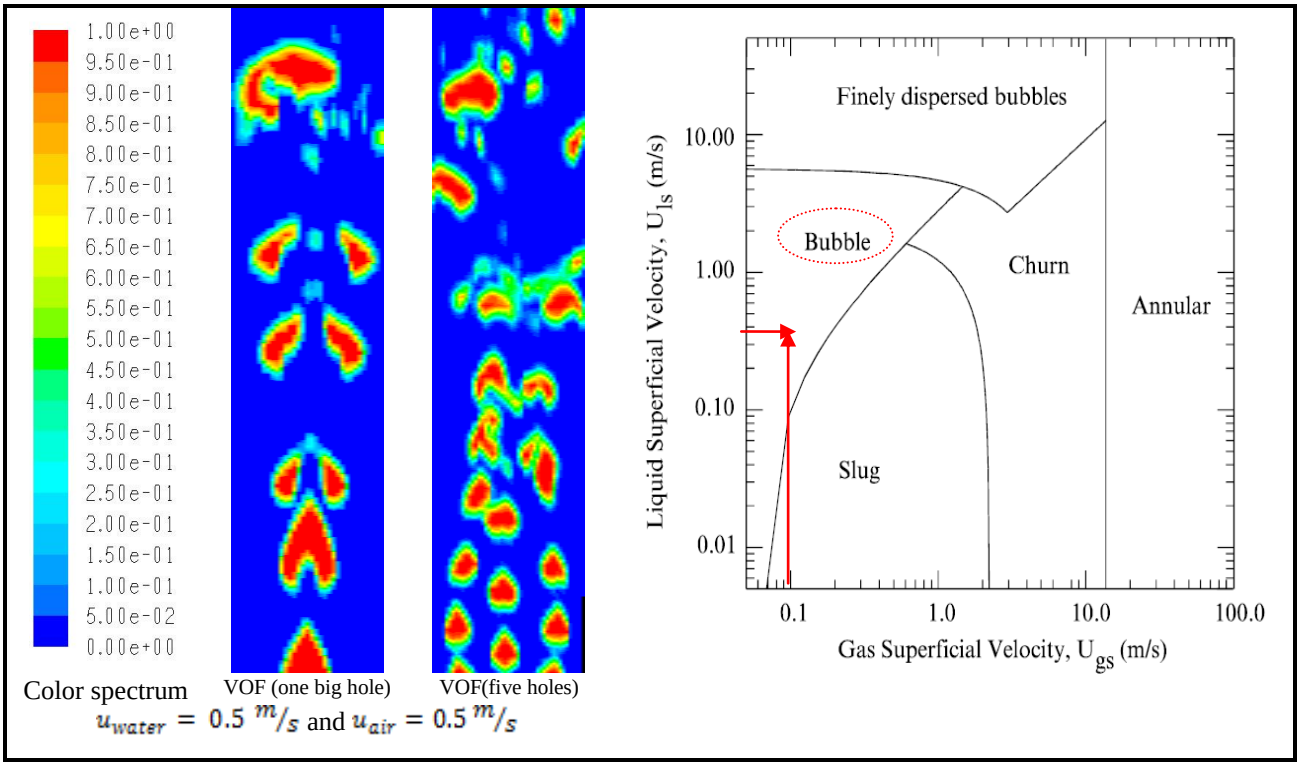


**Fig.13.** Comparisons of VOF and Eulerian methods

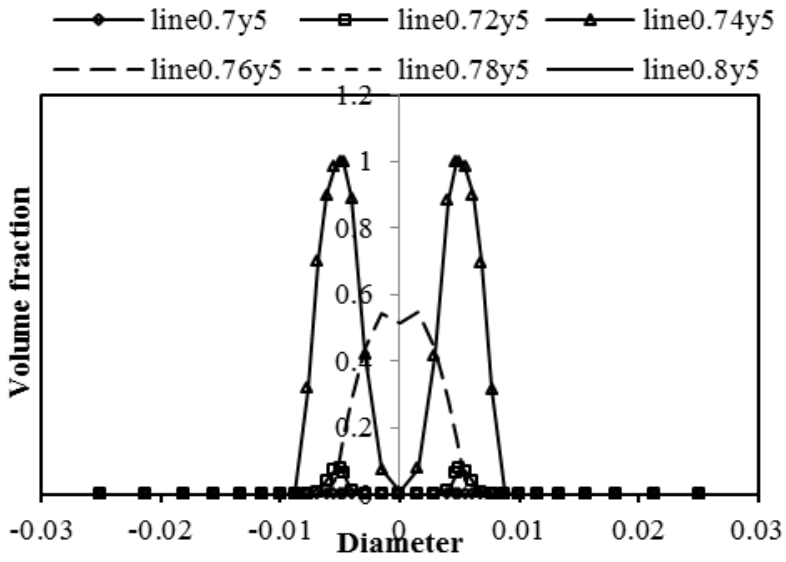


**Fig.14.** Variation of volume fraction in height of o.7m to 0.8m for one hole injection port

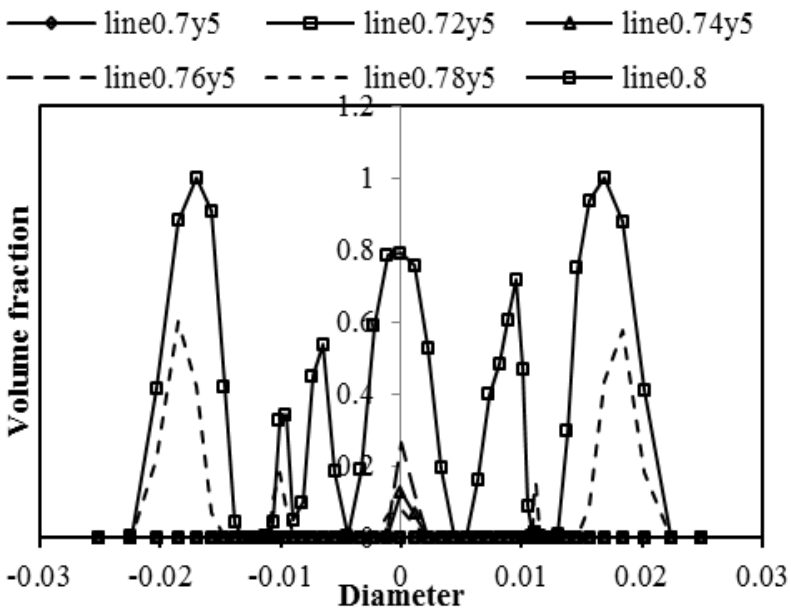


**Fig.15.** Variation of volume fraction in height of o.7m to 0.8m for five holes injection port

Figure 16 compares the simulation of VOF for phase diagram of slug and churn flow regimes in different inlet velocities. The water and air inlet velocities for slug flow are 0.5 and 2 m/s while the same for churn flow are 2 and 4 m/s respectively. It is crystal clear that the VOF can simulate both flow regimes. The superficial velocities of air and water phases for slug flow are, $J_g$ = 0.3974 m/s and $J_f$ = 0.4004 m/s respectively, and for churn flow, $J_g$ =0.7949 m/s and $J_f$ = 1.601 m/s.

Figure 17 displays the phase contours of VOF model for one and five holes injection in inlet air and water velocities of 6 and 2 m/s, respectively. The VOF model nearly could predict the regime. As the figure shows the simulated regime for one hole injection port is more like the real churn flow in the upriser pipe of the airlift pump than the five holes one. It seems that when the regime is situated in the intersection of flow regimes, VOF model also cannot predict and show the

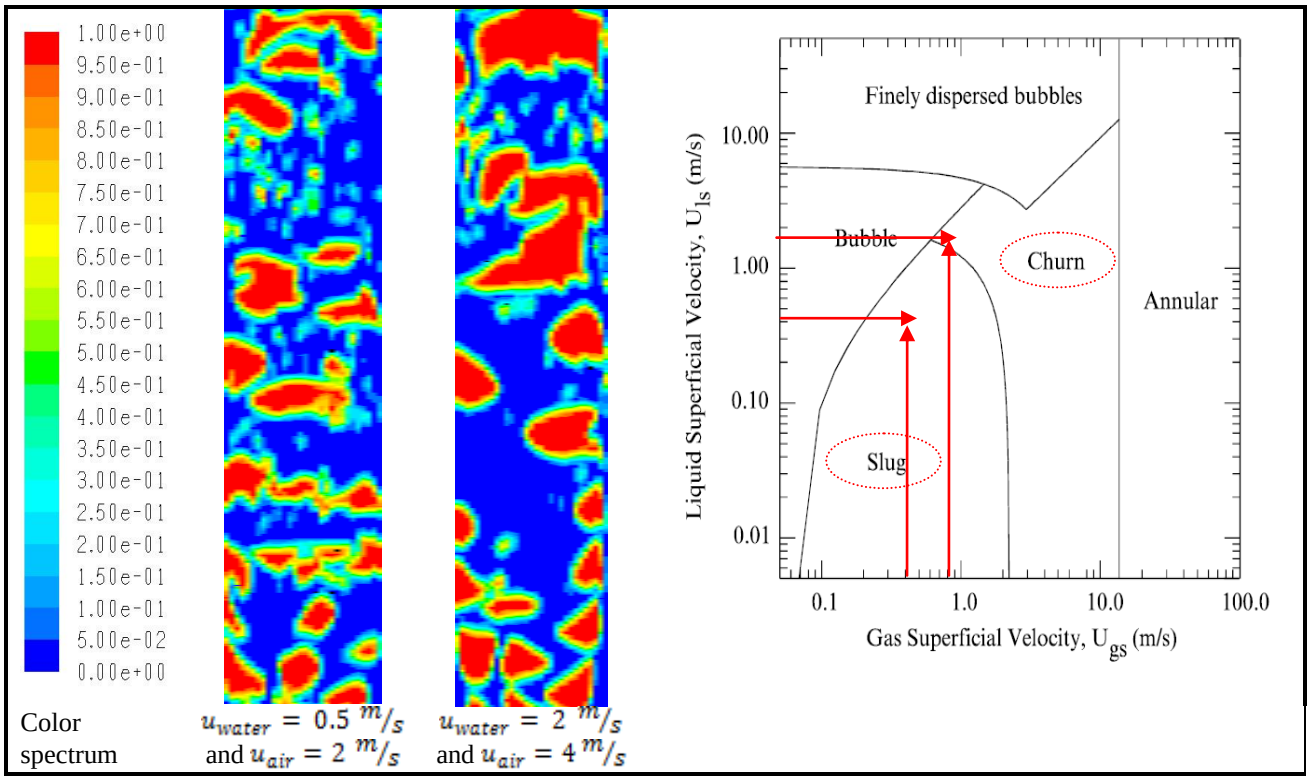


**Fig.16.** Comparison of VOF simulations for slug and churn flow in 5 holes air injection port

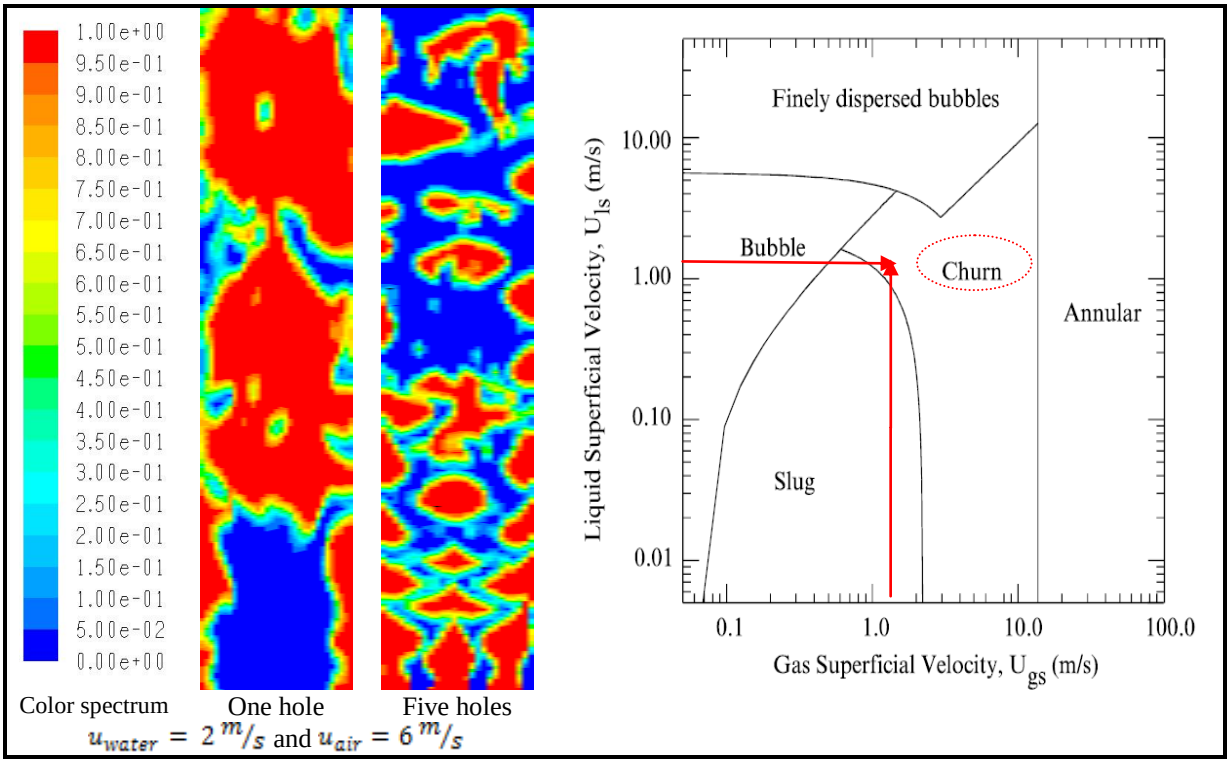


**Fig.17.** Comparison of VOF simulations for one and five holes air injection port in churn flow regime

regime well. The superficial velocities of air and water phases are 1.192 and 1.601 m/s respectively. The map shows that the respective flow regime is churn which corresponds to the simulation.

Figures 18 and 19 show the variation of volume fraction on diameter of the pipe in different height positions in range of 0.7 to 0.8 m for one and five air injection ports. As the figures denote, there are bubbles in different height of the pipe with a high volume fraction.

There are significant increases in value of volume fractions of all these curves in comparison to the previous curves.

It means the amount of air phase in this flow regime is high. Furthermore, figures indicate that air phase almost symmetrically has been distributed. The air phase in one hole injection port concentrates more in the center of the pipe than the five holes.Comparison of the VOF prediction for slug, bubbly and churn flows with photos taken from the experimental setup are denoted in Figs. 20 to 22.

The pictures were taken with a high speed camcorder with 1200 fps. These figures show that the VOF model can fairly predict the shape of the bubble and slug, but the interface of the two phases are not exactly distinguishable.

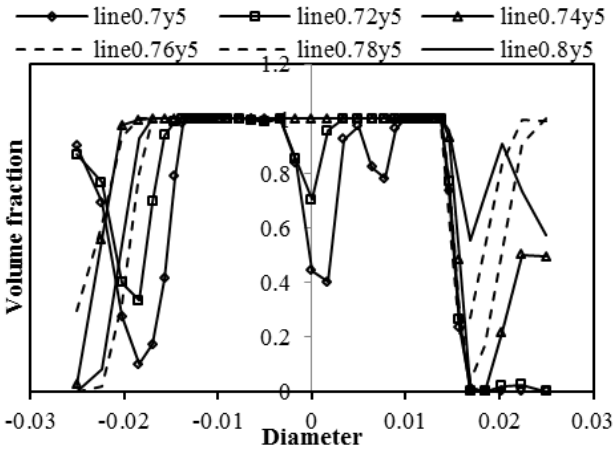


**Fig.18.** Variation of volume fraction in height of o.7 to 0.8 m for one hole air injection port

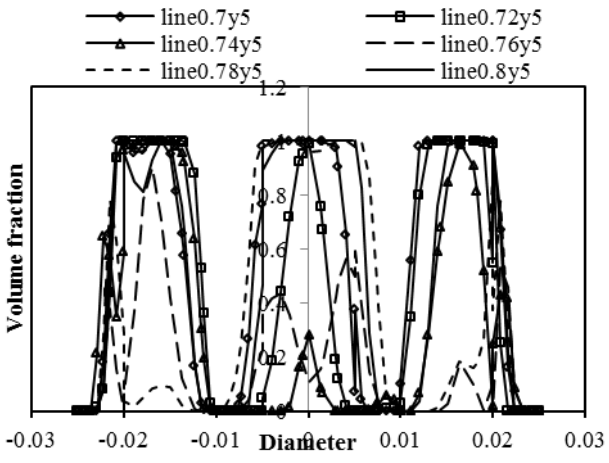


**Fig.19.** Variation of volume fraction in height of o.7 to 0.8 m for five holes air injection port

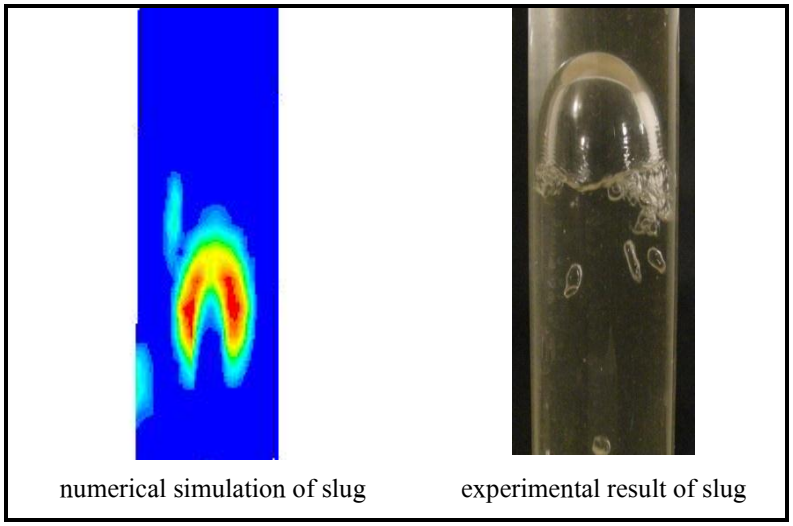


**Fig.20.** Comparison of slug's experimental and numerical result

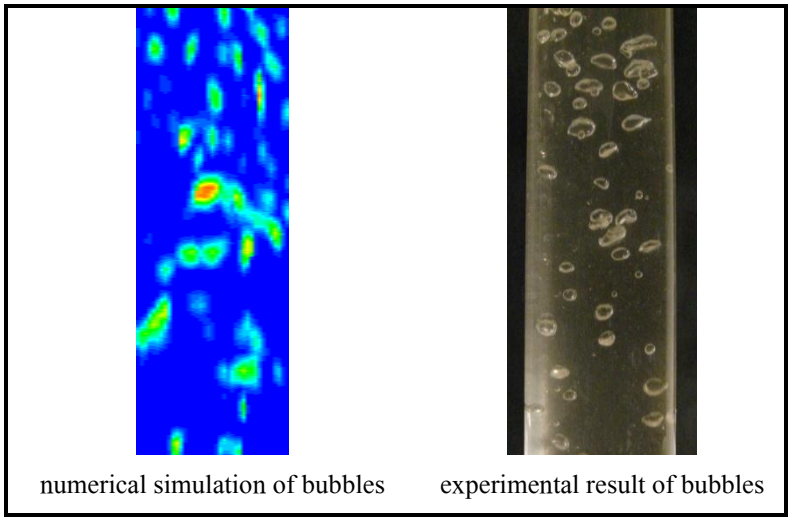


**Fig.21.** Comparison of bubbles' experimental and numerical results

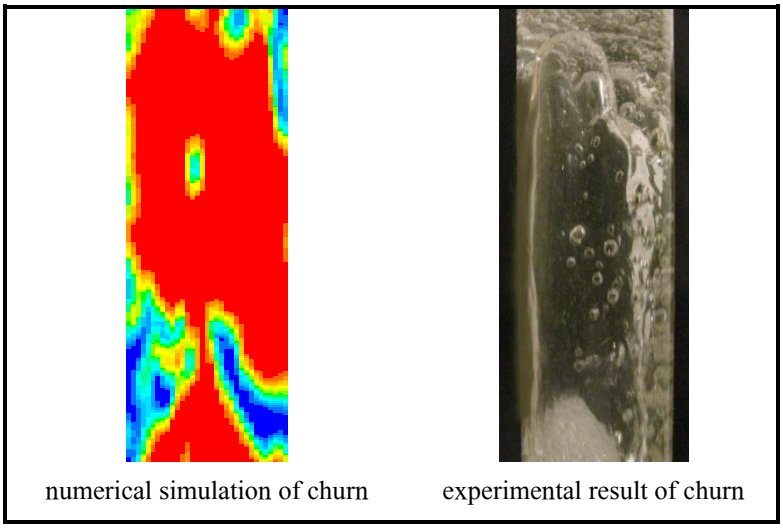


**Fig.22.** Comparison of churn's experimental and numerical results

## 7. Conclusion

In this study, the volume of fluid (VOF) and Eulerian models are used for modeling of the air- water two phase flow in the upriser pipe of the airlift systems. Several velocities were considered for the inlet of the air and water to create the various gas- liquid two phase flow regimes in the pipe and also three sets of inlet geometries were implemented.

The results show that the VOF method is more appropriate for simulating the bubbly, slug and churn flow regime of gas- liquid two phase flow while the annular flow regime is fairly good predicted with Eulerian method. The VOF model is able to simulate the interface of the phases more reliable than the Eulerian one. In the Eulerian model, the separate bubbles were considered as a unified region with lower void fraction. This means that in this model the simulation of the gas phase region is illustrated as a stripe. The color and the width of this stripe depend on the gas phase void fraction. An increase in the mass flow rate of the inlet gas phase increases the gas phase void fraction, and the flow regime changes from bubbly to annular, although providing annular as flow regime needs a very high velocity for all these geometries. The results obtained by geometry including one small hole at the center of the pipe, could not predict some of these regimes at high inlet air velocities. In order to solve this problem and also providing more flow regimes which the previous one could not simulate, the geometries of having 5 holes were used. This geometry presented most of these regimes even better than the previous one because of a good distribution of bubbles in the pipe.

## References


[1] Reinemann, D.J. A theoretical and experimental study of airlift pumping and aeration with reference to aquacultural applications, Doctoral dissertation, Cornell University (1987).

[2] Hanafizadeh, P., Ghorbani, B., Review study of airlift pumping systems, Multiphase Science and Technology, 24 (4): 323-362 (2012) .

[3] Giot, M. Three phase flow, Handbook of multiphase systems, edited by G. Hetsroni, Hemisphere, McGraw Hill (1982).

[4] Kato, H., Miyazawa, T., Timaya, S., and Iwasaki, T. A study of an airlift pump for solid particles, Bull. JSME 18: 286-294 (1975).

[5] Gibson, A., H. Hydraulics and its applications, 5th Edition, Constable, London (1961).

[6] Mero, J. L., Seafloor minerals, A Chemical Engineering Challenge, Chem. Eng. J. 43 (2): 73 (1968).

[7] Chisti, Y. Assure bioreactor sterility, Chem. Eng. Prog. 88(9): 80 (1992).

[8] Trystam, G. and Pigache, S. Modeling and simulation of a large scale air lift fermenter, Proc. Eur. Symp. Comp.-Aid. Proc. Eng.-2: 5171-5176 (1992).

[9] Abed, K., A. Theoretical study on the performance of airlift pumps, The Institution of Engineers, MC, 77: 202 (1977).

[10] White, E. T., and Beardmore, R. H.The velocity of rise of single cylindrical airbubblesthrough liquids contained in vertical tubes, Chem. Eng. Sci. 17: 351-361 (1962).

[11] Zukoski, E. E. Influence of viscosity, surface tension, and inclination angle on motion oflong bubbles in closed tubes, J. Fluid Mech. 20: 821-832 (1966).

[12]Kouremenos, D., A., and Staicos, J. Performance of a small air-lift pump. Int. J. Heat Fluid Flow 6: 217-222 (1985).

[13]Zenz, F.A. Explore the potential of air-lift pumps and multiphase systems, Chem. Eng. Prog., 89(8), p. 51 (1993).

[14] De Cachard, F. and Delhaye, J. M. A slug-churn model for small-diameter airlift pumps, Int. J. Multiphase Flow, 22 (4): 627-649 (1996).

[15] De Cachard, F., and Delhaye, J. M. Stability of small diameter of airlift pumps, Int. J. Multiphase Flow, 24 (1), pp. 17-34 (1998).

[16] Geest, S., van., Ellepola, J., H. and Oliemans, R.V.A. Comparisonof different air injectionmethods to improve gas-lift performance,Proceedings of the 10th Conference Multiphase 01, France (2001).

[17] Guet, S., Ooms, G. and Oliemans, R. V. A. Influence of bubble size on the transition fromlow-re bubbly flow to slug flow in a vertical pipe, Experimental Thermal and Fluid Science, 26 (6): 635–641 (2002).

[18] Kassab, S. Z., Kandil, H. A.,Warda, H. A., and Ahmed, W. H. Air-lift pumps characteristics under two-phase flow conditions, Int. J. Heat and Fluid Flow, 30: 88-98 (2009).

[19] Hanafizadeh, P., Ghanbarzadeh, S., and Saidi, M.H. Visual technique for detection of gas- liquid two phase flow regime in the airlift pump, Journal of Petroleum Science and Engineering, 75, pp. 327-335 (2011).

[20] Hanafizadeh, P., Saidi, M. H., Darbandi, M., Kebriae, A. Numerical simulation of two-phase flow in airlift pumps using the physical influence scheme, Progress in Computational Fluid Dynamics; an International Journal, 10 (3), pp.186- 194 (2010).

[21] Hanafizadeh,P., Karimi, A., and Saidi, M.H. Effect of step geometry on the performance of the airlift pump, International Journal of Fluid Mechanic research, 38 (5), pp. 387- 408 (2011).

[22] Simonin, O. Eulerian formulation for particle dispersion in turbulent two-phase flows, Proc. of the 5thWorkshop on Two-Phase Flow Predictions, Erlangen, Germany (1990).

[23] Hanafizadeh,P., Karbalaee, M.S., Sharbaf, E.B., Ghanbarzadeh,S., Drag coefficient and strouhal number analysis of cylindrical tube in two phase flow, Journal of Energy Equipment and Systems, Vol. 1, pp. 34-95 (2013).

[24] Brackbill, J., U., Kothe, D., B., and Zemach, C. A continuum method for modeling surface tension,

J. Comput. Phys., 100:335-354 (1992).
[25] Drew, D., A., and Lahey. R., T. In particulate two-phase flow, pages 509-566. Butterworth-Heinemann,Boston (1993).
[26] Sato, Y., and Sekoguchi, K. Liquid velocity distribution in two-phase bubbly flow, Int. J. Multiphase Flow 2: 79–95 (1975).
[27] Launder, B., E., Spalding, D., B. Mathematical models of turbulence, GB: Academic Press, London (1972).
[28] Csanady, G. T. Turbulent diffusion of heavy particles in the atmosphere, J. Atmos. Science 20: 201-208 (1963).
[29] Patankar, S. V. Numerical heat transfer and fluid flow, McGraw-Hill, New York (1980).
[30] Fogt, H., and Peric, M. Numerical calculation of gas- liquid flow using a two- fluid finite volume method, Numerical Method in Multiphase Flows, 185, pp. 73-80 (1994).
[31] Taitel, Y., Barnea D. and Dukler, A.E. Modeling flow pattern transitions for steady upward gas-liquid flow in vertical tubes,AIChE J., 26, 345-354 (1980).